TECHNICAL MEMORANDUM

ANL-OTEC-78-2
Distribution Category UC-64

VAPOR/LIQUID INTERACTION AND ENTRAINMENT IN SHELL-AND-TUBE EVAPORATORS

by

D. Yung, J. J. Lorenz, and E. N. Ganic

Components Technology Division
Argonne National Laboratory

USDOE Division of Solar Energy

June 1978

DISCLAIMER

The facilities of Argonne National Laboratory are owned by the United States Government. Under the terms of a contract (W-31-109-Eng-38) between the U. S. Department of Energy, Argonne Universities Association and The University of Chicago, the University employs the staff and operates the Laboratory in accordance with policies and programs formulated, approved and reviewed by the Association.

MEMBERS OF ARGONNE UNIVERSITIES ASSOCIATION

The University of Arizona
Carnegie-Mellon University
Case Western Reserve University
The University of Chicago
University of Cincinnati
Illinois Institute of Technology
University of Illinois
Indiana University
Iowa State University
The University of Iowa
Kansas State University
The University of Kansas
Loyola University
Marquette University
Michigan State University
The University of Michigan
University of Minnesota
University of Missouri
Northwestern University
University of Notre Dame
The Ohio State University
Ohio University
The Pennsylvania State University
Purdue University
Saint Louis University
Southern Illinois University
The University of Texas at Austin
Washington University
Wayne State University
The University of Wisconsin

TECHNICAL MEMORANDUM

ANL-OTEC-78-2
Distribution Category UC-64

VAPOR/LIQUID INTERACTION AND ENTRAINMENT IN SHELL-AND-TUBE EVAPORATORS

by

D. Yung,* J. J. Lorenz,* and E. N. Ganic†

Components Technology Division
Argonne National Laboratory

USDOE Division of Solar Energy

June 1978

*Argonne National Laboratory, Components Technology Division

†University of Illinois at Chicago Circle, Department of Energy Engineering

Table of Contents

List of Figures

NOMENCLATURE

A	column cross-sectional area, m^2
C_1	constant, Eq. (2)
C_d	vapor drag coefficient
d	droplet diameter, m
d^*	effective column diameter, Eq. (15), m
D	tube diameter, m
f	capillary wave oscillation frequency, s^{-1}
F_d	vapor drag force, N
g	gravitational acceleration, m/s^2
L	column length, m
m	droplet mass, kg
M	mass of both primary and secondary droplets, kg
P	tube pitch, m
S	tube spacing, m
t	time, s
u	velocity, m/s
V	column volume, m^3
W	column weight, kg
We	Weber number, Eq. (9)
x	coordinate, Fig. 4, m
y	coordinate, Figs. 4 and 6, m
z	coordinate, Fig. 6, m

Greek letters

α	deflection angle, rad
ζ	fraction of blocked area
θ	critical deflection angle, Eq. (4), rad
λ	wave length, Eq. (1), m
μ	viscosity, $N \cdot s/m^2$
ρ	density, kg/m^3
σ	surface tension, N/m
Γ	flowrate, $kg/s \cdot m$

NOMENCLATURE (contd.)

Subscripts

c	critical
g	gas or vapor
ℓ	liquid
p	primary
s	secondary

ABSTRACT

The problem of vapor/liquid interaction and entrainment in shell-and-tube evaporators is analyzed. Attention is focused primarily on the horizontal tube falling film evaporators, which have been proposed for use in Ocean Thermal Energy Conversion (OTEC) power plants. In the horizontal tube design, liquid falls from one tube to the next in either a droplet or column mode. A criterion is derived for predicting the transition from the droplet mode to the column mode. Models are developed for predicting the deflection of droplets and columns due to vapor crossflow. Based on an experimental study of drop detachment and breakup, a correlation is established for determining the resulting droplet sizes. For high vapor crossflow velocities, a criterion is presented for predicting the inception of liquid entrainment by a process known as stripping. Based on the foregoing models, conditions are defined under which vapor/liquid interaction and entrainment are important for OTEC evaporators.

1.0 INTRODUCTION

An evaporator concept widely used in desalination systems and recently proposed for use in Ocean Thermal Energy Conversion (OTEC) power plants is the shell-and-tube design, where a thin film of working fluid is evaporated on either horizontal or vertical tubes. With these types of designs, vapor crossflow may cause serious problems, such as redistribution of the working fluid and incomplete wetting of tubes. Reliable evaporator design requires a clear understanding of the effect of vapor crossflow. The purpose of this paper is to study the basic mechanisms of vapor/liquid interaction and entrainment and to develop models applicable to the design and performance evaluation of shell-and-tube evaporators for OTEC.

Compared to the vertical configuration, the horizontal design is considerably more vulnerable to vapor/liquid interaction. Thus attention is focused primarily on the latter design. In a typical horizontal tube falling film evaporator, working fluid is fed at the top of vertical banks of horizontal tubes. In the absence of vapor crossflow the unevaporated fluid from any given tube will fall onto the next lower tube, and the qualitative structure of the falling liquid is dependent primarily on the feed flowrate. At relatively low feed flowrates the fluid falls from one tube to the next in the form of droplets, which are created by Taylor instabilities along the bottom portion of the tubes, see Fig. 1a. At higher feed flowrates a transition region is encountered where intermittent droplets and columns are formed. Upon increasing the flowrate still further a critical flowrate is reached beyond which the liquid falls as stable columns, Fig. 1b. At extemely high feed flowrates the liquid falls as unstable sheets and columns, but these high flowrates are generally outside the range of interest for OTEC.

As a result of vapor crossflow the droplets and columns falling from a given tube may be partially or totally deflected away from the next lower tube, thereby causing liquid redistribution and incomplete wetting of lower tubes in the bank. In addition to these deflection mechanisms, a number of entrainment mechanisms can also occur. For example if nucleate boiling is present in the film, a mist of small droplets is generated as bubbles burst through the film, and the small droplets are readily entrained by the flowing vapor. An entrainment mechanism common to both horizontal and

vertical designs is that of shearing or "stripping" of the thin liquid film from the tube surface. In this paper models of the foregoing mechanisms, among others, are developed. Based on the models, conditions are defined under which vapor/liquid interaction and entrainment are important for OTEC. Whenever an example is given for OTEC, ammonia is assumed to be the working fluid.

Simple experiments have also been conducted to study the dynamics of drop formation and breakup. Results from such experiments provide some of the necessary information for the development of the present models.

2.0 MODELLING

The following models generally apply to horizontal tube falling film evaporators which are the most vulnerable to vapor/liquid interaction. It will be clearly stated when the models apply to other evaporator designs.

2.1 Droplet Mode. In a horizontal tube evaporator, the physical form of the liquid flowing from one tube to the next depends on the liquid flowrate and the distance between the tubes. When the flowrate is small and the tube spacing is large, the liquid is usually in the form of droplets. If the flowrate is large or the tube spacing is small, the liquid may flow in the form of columns. The criterion for the transition from the droplet mode to the column mode will be discussed in the next section.

In the droplet mode, droplets are produced from discrete points along the underside of the horizontal tube. The present problem of a thin film on the underside of a horizontal tube relates to a classic hydrodynamics problem known as Taylor instability [1], see Fig. 2. Taylor instability states that when a heavier fluid is on top of a lighter fluid, such as liquid over vapor in the present case, the system is not stable. Taylor instability also states that the instability wave that will most likely appear at the interface has a wave length:

$$\lambda = 2\pi\sqrt{\frac{3\sigma}{\rho_\ell g}} \tag{1}$$

where σ and ρ_ℓ are the surface tension and density of the fluid, respectively, and g is the gravitational acceleration. Since the formation of droplets in the present case is a result of the growth of an instability wave at the interface, it is reasonable to expect that the spacing between the droplet generation sites is equal to the wavelength λ given by Eq. (1). (It should be pointed out that Eq. (1) has successfully been used to predict the spacing between vapor bubble columns in stable film boiling [2, 3].) For ammonia at 22°C (72°F), Eq. (1) predicts a wavelength of 2.0 cm (0.8 in.) which is in good agreement with the experimentally measured spacing of 1.9 cm (0.75 in.) by Sabin and Poppendiek [4]. Furthermore Eq. (1) was found to agree reasonably well with our experiments with ethyl alcohol, which will be discussed shortly.

The mechanism of detachment of a drop from a liquid film is extremely difficult to treat analytically. To study the detachment mechanism,

a simple experiment was performed with ethyl alcohol, which was chosen because of its similarity to ammonia in wettability, surface tension, and density. Ethyl alcohol at room temperature (20°C) was fed from a buret onto an unheated 3.8 cm (1.5 in.) diameter horizontal aluminum tube. The liquid droplets from the underside of the tube were photographed by a high speed camera at 200 frames/sec. Figure 3 shows a sequence of photographs of a detaching drop. As a drop detaches from the film, it carries with it a long narrow tail, which, by the well known Rayleigh instability, eventually breaks up into 4 or 5 smaller droplets. A slight increase in drop size with the flowrate was observed (the variation in size is usually within ± 5% of its nominal value). Also the length of the tail increased with flowrate. The large drop in Fig. 3 will be referred to as the primary drop, and the 4 or 5 smaller drops as secondary drops. The mechanism by which the liquid breaks off from the film is essentially an interaction of gravity and surface tension forces. It is reasonable to expect that the diameter, d_p, of a primary drop can be correlated by an expression such as:

$$d_p = C_1\sqrt{\frac{\sigma}{\rho_\ell g}} \tag{2}$$

where C_1 is a constant. The value of the constant C_1 was determined from our experiments with alcohol to be 2.7. The secondary drops could also be correlated by a similar expression but with different constants. However, it was decided to express the diameter, d_s, of the secondary drops in terms of the ratio d_s/d_p. From the experimental data it was found that:

$$0.23 < \frac{d_s}{d_p} < 0.38 \tag{3}$$

It was estimated that the volume of the secondary droplets compared to the total volume of droplets is about 10%. It is expected that Eq. (2) and expression (3) can be applied to any good wetting fluid. For ammonia at 22°C (72°F) the foregoing expressions predict d_p = 5.1 mm (0.20 in.) and 1.2 mm (0.05 in.) < d_s < 1.9 mm (0.08 in.). These predicted drop sizes are consistent with experimentally measured drop sizes for ammonia [4].

Knowing the drop sizes, it is possible to calculate the droplet deflections due to vapor crossflow. In Fig. 4 the angle α is the actual drop deflection angle and θ is the critical angle beyond which the drop will not hit the lower tube. Deflection angles for which $\alpha < \theta$ are considered safe in

the sense that the drop will hit the lower tube, although it is recognized that non-uniform wetting of the lower tube may still result. The angle θ has a simple relationship to the pitch-to-diameter ratio P/D as

$$\theta = \tan^{-1}\left\{\frac{1}{2}\left[\frac{P}{D}\left(\frac{P}{D} - 1\right)\right]^{-\frac{1}{2}}\right\} \tag{4}$$

Further remarks concerning θ and P/D will be given in a later section on tube arrangement.

Based on the coordinates shown in Fig. 4, the equations of motion of a single droplet, in the presence of vapor crossflow velocity u_g, are:

<u>x-direction</u>
$$m\frac{d^2x}{dt^2} = C_d\left(\frac{\pi d^2}{4}\right)\frac{1}{2}\rho_g u_g^2 \tag{5}$$

<u>y-direction</u>
$$m\frac{d^2y}{dt^2} = m\,g \tag{6}$$

where m and d are the mass and diameter of the droplet, respectively, ρ_g is the vapor density and C_d is the drag coefficient. Certain assumptions are implied in the formulation of the above equations. These assumptions are: (1) the motion of the droplet in the y direction is mainly governed by gravity (i.e., vapor drag force in that direction is small); and (2) the motion of the droplet in the x direction is mainly due to the vapor drag force at a steady vapor crossflow velocity u_g (i.e., the reduction in drag force due to the motion of the droplet in the x direction is small). Without these assumptions, the formulation given by Eqs. (5) and (6) would be much more complex because the vapor flow around the droplet is basically non-steady. With these assumptions, the problem is reduced to a steady state flow problem with known values for the drag coefficient C_d. It is realized that these assumpitons are valid only if the error introduced is small. This, however, is found to be true as will be discussed later when the solution is applied to a typical ammonia droplet case.

The drag coefficient C_d in Eq. (5) depends generally on the Reynolds number of the vapor flow. Equation (5) can be further simplified by restricting our solution to Reynolds number greater than 1000, which is usually the case. At Reynolds number between 10^3 and 10^5, the drag coefficient has a simple value of 0.44 [5].

The boundary conditions for Eqs. (5) and (6) are $x = dx/dt = y = dy/dt = 0$ at $t = 0$. In setting $dy/dt = 0$ at $t = 0$, it is somewhat conservatively assumed that the droplet has no initial velocity as it departs from the tube. Equations (5) and (6) indicate that the trajectory of a deflected droplet is a straight line. The angle of deflection α, defined as $\alpha = \tan^{-1}(x/y)$, can be easily obtained from Eqs. (5) and (6) as

$$\alpha = \tan^{-1}\left\{\frac{1}{3}\,\frac{\rho_g}{\rho_\ell}\,\frac{u_g^2}{d\,g}\right\} \tag{7}$$

The critical vapor crossflow velocity u_g for which the droplet deflection angle α is equal to the maximum allowable angle θ, can be obtained by combining Eqs. (4) and (7) into:

$$u_g = \left\{\frac{3}{2}\,\frac{(\rho_\ell/\rho_g)\,d\,g}{\sqrt{(P/D)[(P/D) - 1]}}\right\}^{\frac{1}{2}} \tag{8}$$

Equation (8) is plotted in Fig. 5 for the case of ammonia droplets at a temperature of 22°C (72°F). In Fig. 5, the critical ammonia vapor crossflow velocity u_g is plotted as a function of typical ammonia droplet diameters d, and for various typical pitch-to-diameter ratios P/D. The dash region for small drop diameters indicates a range where Eq. (8) is not strictly applicable because the Reynolds number is less than 1000; thus the curves are only projected values. The atomization region in Fig. 5 indicates an area where droplets would not be able to exist because of disintegration due to high vapor velocity. The atomization boundary is based on a Weber number of 12 [6], where the Weber number is defined as:

$$We = \frac{\rho_g\,u_g^2\,d}{\sigma} \tag{9}$$

The diameter d in this equation defines the maximum drop size that can exist for a given crossflow velocity. A drop which is larger than the maximum drop size corresponding to a given vapor velocity can disintegrate into many smaller droplets. Although the curves in Fig. 5 are obtained from a simplified set of equations, the results are quite accurate. From a slightly more involved analysis, it was found that the calculated vapor velocity may be slightly higher than the true value. If the tube spacing is less than 2.5 cm (1 in.), the overestimate is at most 20%.

The safe region in Fig. 5 is the area for which $\alpha < \theta$ (to ensure that the droplet hits the lower tube) and lying below the atomization boundary

(to avoid potential disintegration into much smaller droplets that can easily be deflected). For a given P/D, the intersection of Eqs. (8) and (9) defines the maximum allowable crossflow velocity. For P/D = 1.25 this maximum velocity is 2.9 m/s and occurs at d = 3.8 mm. Recall that the predicted drop sizes for ammonia are d_p = 5.1 mm and 1.2 mm < d_s < 1.9 mm. From Fig. 5 for P/D = 1.25 the corresponding maximum velocities are 2.6 m/s for the primary drop and 1.6 m/s to 2.1 m/s for the secondary drops. If the crossflow velocities are kept below 1.6 m/s no droplets will be deflected away from lower tubes although non-uniform tube wetting may occur. For crossflow velocities in the range 1.6 m/s to 2.1 m/s, some of the secondary droplets will be deflected from the lower tube and will strike a tube in the next column. At 2.1 m/s all the secondary drops are deflected, representing 10% of the liquid falling from the tube. Velocities beyond 2.6 m/s may cause disintegration of primary droplets into much smaller droplets, thus potentially causing 100% deflection of liquid from the lower tubes.

Based on the preceeding example, it was seen that vapor crossflow can produce partial or total deflection of droplets from the lower tubes. This can lead to non-uniform and incomplete wetting of tubes, and redistribution of working fluid from one column to the next. The net effect is a loss in heat transfer performance. To completely avoid deprivation of liquid to the lower tubes and redistribution of working fluid, the crossflow velocity should not exceed 1.6 m/s. However even under these conditions it should be recognized that non-uniform tube wetting can still occur. It should also be pointed out the largest crossflow velocities occur in the outermost regions of an evaporator unit. For large bundle evaporators, therefore, vapor lanes should be considered to reduce vapor velocity so as to avoid the aforementioned liquid deflection and entrainment problems.

2.2 Column Mode. An expression for the critical flowrate above which stable columns are formed was obtained by setting the droplet production frequency equal to the capillary wave oscillation frequency at the film interface, yielding:

$$\Gamma_c = \frac{M f}{\lambda} \tag{10}$$

where λ is the Taylor wave length given by Eq. (1), M is the mass of all the droplets in each drop breakup, and f is the critical breakup frequency.

The total droplet mass, M, is simply:

$$M = 1.1\ \rho_\ell \frac{\pi\ d_p^3}{6} \tag{10a}$$

where d_p is the primary droplet diameter given by Eq. (2)* and the factor of 1.1 accounts for the mass of all the secondary droplets. The critical breakup frequency is simply that of the capillary wave oscillation frequency at the film surface, which is [7]

$$f = \sqrt{\frac{2\pi\ \sigma}{\rho\ \lambda^3}} \tag{10b}$$

This assumes that after each drop breakup, the film surface bounces once, at the characteristic speed of a capillary wave, before another drop can be formed, and that the maximum breakup frequency is limited by the capillary wave oscillation frequency given by Eq. (10b). Note that for flowrates smaller than Γ_c, the drop breakup frequency can be smaller than the capillary wave oscillation frequency. For flowrates greater than Γ_c, droplet mode is not possible and the flow changes to the column mode. Equation (10) is in good agreement with the experimentally observed critical flowrates for ethyl alcohol. Applying Eq. (10) to ammonia at 22°C (72°F), the critical flowrate above which columns will form is about 0.013 kg/s·m (32 lb/hr-ft).

Figure 1b shows a sketch of the fully developed column mode. As in the case of droplets, the column spacing will be prescribed by the most unstable wavelength, λ, from Eq. (1). A liquid column has a tapered shape but for analytical purposes it is convenient to model the column as a right circular cylinder having the same length and an effective diameter, d^*, such that the volumes are equivalent. The effective diameter is determined as follows. Referring to Fig. 6a, the velocity at any position y below the tube is given by the "free-fall" expression:

$$u_\ell = \sqrt{2\ g\ y} \tag{11}$$

Here it is conservatively assumed that the liquid velocity at y = 0 is negligibly small. The mass flowrate for a single column is $\lambda\Gamma$, where λ is

*For the calculation of d_p we recommend using $C_1 = 2.83$ instead of 2.7 because the drop sizes at flowrates approaching transition were 5% larger than nominal.

column spacing and Γ is the liquid flowrate per unit length. Employing the foregoing in conjunction with the continuity equation, the following expression for the column cross-sectional area is obtained:

$$A = \frac{\lambda \Gamma}{\rho_\ell \sqrt{2 g y}} \tag{12}$$

from which the column volume V can be determined by integration. Substituting $y = z \cos \alpha$ and integrating from $z = 0$ to L yields:

$$V = \int_0^L A \, dz = \frac{2 \lambda \Gamma \sqrt{L}}{\rho_\ell \sqrt{2 g \cos \alpha}} \tag{13}$$

Then the effective diameter is determined from:

$$\left(\frac{\pi d^{*2}}{4}\right) L = V \tag{14}$$

Upon substituting V from Eq. (13) and letting $L = S/\cos \alpha$, the effective diameter can be expressed as:

$$d^* = \left(\frac{8 \lambda \Gamma}{\pi \rho_\ell \sqrt{2 g S}}\right)^{\frac{1}{2}} \tag{15}$$

Referring to Fig. 6b, the column deflection angle, α, due to vapor cross-flow can be determined from a balance of forces normal to the cylinder:

$$F_d = W \sin \alpha \tag{16}$$

where F_d is the drag force based on the component of velocity normal to the cylinder:

$$F_d = C_d L d^* \frac{\rho_g}{2} (u_g \cos \alpha)^2 \tag{16a}$$

and W is the weight of the column:

$$W = \rho_\ell g V \tag{16b}$$

After making the appropriate substitutions into Eq. (16) and with some rearrangement the following expression is obtained:

$$\frac{C_d d^* \rho_g u_g^2 \sqrt{2 g S}}{4 \lambda \Gamma g} = \frac{\tan \alpha}{\cos \alpha} \tag{17}$$

where d^* is defined by Eq. (15) and λ by Eq. (1).

The critical angle θ beyond which the column will no longer hit the next lower tube is given the same expression as for drops, i.e., Eq. (4). Substituting θ for α in Eq. (17) leads to an equation defining the critical condition for columns. For this condition, Eq. (17) is plotted in Fig. 7 as u_g vs Γ for various P/D ratios. The calculations are for ammonia at 22°C (72°F). The between-tube distance S was determined by assuming 5.1 cm (2 in.) diameter tubes. It is easy to show that $u_g \sim S^{-1/8}$ and consequently the results are not sensitive to S. The drag coefficient over the Reynolds numbers of interest is $C_d = 1$.

In Fig. 7 the "safe" region is the area for which $\alpha < \theta$ (to ensure that the column hits the lower tube). Only the region for which $\Gamma \geq \Gamma_c$ is considered since the droplet mode dominates for $\Gamma < \Gamma_c$. For $\Gamma = \Gamma_c$ and P/D = 1.25, the maximum allowable crossflow velocity is $\sim$ 1.5 m/s (5 ft/sec). This velocity is roughly the same as the maximum allowable crossflow velocity for the smallest secondary drops found in the droplet mode, see previous section. As Γ increases, the column thickens and a higher crossflow velocity is required to deflect the column. At Γ = 0.21 kg/s·m (500 lb/hr·ft), the allowable velocity is about 3 m/s (10 ft/sec). For $\alpha > \theta$ the column will be deflected away from the lower tube and impinge on a tube in the adjacent column of tubes. This leads to deprivation of liquid to the lower tubes and redistribution of the working fluid. To avoid these problems the maximum allowable velocity for a given flowrate Γ should not be exceeded. However even under these conditions it should be recognized that non-uniform tube wetting can still occur.

Before closing this section a simple model will be given for predicting the fraction of the vapor crossflow area which is blocked by liquid columns. Referring to Fig. 1b, the fraction, ζ, of blocked area based on the projected area of the column is

$$\zeta = \frac{d^* S}{\lambda S} = \frac{d^*}{\lambda} \tag{18}$$

where d^* is given by Eq. (15) and λ by Eq. (1). For ammonia, Eq. (18) predicts that $\sim$ 8% of the flow area is blocked at the critical flowrate for column formation. At Γ = 0.21 kg/s·m (500 lb/hr·ft), nearly 30% of the

area is blocked. The percent blocked area will influence the shell-side velocities and pressure drops; and consequently must be carefully considered in the thermal design.

2.3 Stripping. The previous two sections dealt with the deflection of liquid as it falls from one tube to the next. This section considers entrainment phenomena associated with the thin liquid film on the tube surface. The models developed herein apply to both horizontal and vertical tube designs.

In a shell-and-tube evaporator, liquid flows over the tubes in the form of a thin film. If the vapor velocity is sufficiently high, the liquid film becomes unstable as a result of the well known Helmholtz instability [8] phenomenon. The growth of instability waves eventually leads to droplet formation and entrainment. The inception criteria for droplet entrainment in thin films has been considered by numerous investigators. A review paper on this subject was published by Ishii and Grolmes [9]. Ishii and Grolmes proposed new criteria for droplet entrainment in two-phase co-current film flow, which were shown to agree well with all available experimental data. Their inception criteria relate the critical gas velocity (in dimensionless form) to the liquid Reynolds number and the flow direction (whether horizontal, upward, or downward flow). From their inception criteria, the lowest gas velocity to cause entrainment, irrespective of the liquid Reynolds number and flow direction, is given by:

$$\frac{u_g}{\sigma}\sqrt{\frac{\rho_g}{\rho_\ell}}\left\{\frac{\mu_\ell \rho_\ell^2 \sigma^3}{(\rho_\ell-\rho_g)g}\right\}^{\frac{1}{5}} = 1 \qquad (19)$$

where μ_ℓ is the liquid viscosity. Although Eq. (19) is strictly applicable only to co-current gas-liquid flow it should also apply to counter-current flow when the liquid velocity is small compared to the critical vapor velocity. In both horizontal and vertical evaporators for OTEC, the condition of small liquid velocity is satisfied and hence Eq. (19) is generally applicable.

When the gas density is much smaller than the liquid density, $\rho_g \ll \rho_\ell$, the left hand side of Eq. (19) can be rearranged into a ratio of two important similarity parameters: the Kutateladze number [10] and the Kapitza number [11]. The Kutateladze number represents the ratio of the disturbance force (gas velocity) to the restoring force (surface tension) at the interface, and is an important parameter in the study of two-phase interfacial stability problems [10]. The Kapitza number relates to the

internal stability of the liquid film and is an important parameter in the study of thin liquid film flows [11]. Based on the foregoing remarks, the inception criterion expressed by Eq. (19) is seen to have a straight forward physical interpretation.

For ammonia at 22°C (72°F), Eq. (19) indicates a vapor velocity of 4.7 m/s (15 ft/sec). If an evaporator is designed to satisfy the droplet and column deflection constraints discussed in the previous sections, then entrainment by stripping will not be a problem.

2.4 Other Entrainment Mechanisms. In this section two other entrainment mechanisms will be considered, namely those due to nucleate boiling and splashing.

When nucleate boiling is present in the film, a mist of small droplets can be generated as bubbles burst through the film, and the small droplets can readily be entrained by vapor crossflow. Our literature survey revealed only one paper dealing with droplet formation resulting from boiling in thin films [12]. Petrovichev et al. [12] used water as the test fluid, and found that the droplet generation rate depends on both the heat flux and film thickness. What determines the degree of entrainment, of course, is not the total droplet generation rate but rather the ratio of droplet generation rate to the vapor generation rate, a parameter which will be referred to as the droplet entrainment rate. If the Petrovichev correlation is also valid for ammonia, the droplet entrainment rate can be calculated for a typical OTEC ammonia saturation temperature of 22°C (72°F). If we assume a high heat flux of 0.032 MW/m^2 (10^4 $Btu/hr\text{-}ft^2$) and a relatively large film thickness of 0.33 mm (corresponding to a flowrate of 0.2 kg/s·m, or 500 lb/hr·ft), the Petrovichev correlation gives a droplet entrainment rate of only 0.23×10^{-2} (0.23%). However, the Petrovichev correlation may not be valid for ammonia because it is not dimensionless and is therefore not strictly applicable to any fluid except water. For example, it was shown by Newitt et al. [13] that bubble size affects the droplet entrainment rate. Given the fact that ammonia liquid has smaller vapor bubbles than water, the actual droplet entrainment rate may be different from that predicted by the Petrovichev correlation. Consequently further study in this area is needed before any definite conclusions can be reached.

Another possible entrainment mechanism is that due to splashing. Splashing can occur when a liquid impinges onto a solid surface. This process can generate drops of various sizes which are likely to be entrained by the vapor. The extent of splashing depends primarily on wettability and fluid velocity. Experiments with vertical banks of horizontal tubes (simulating an OTEC evaporator) indicated that splashing is not significant when the working fluid adequately wets the tubes [14]. Based on these test results and our own experimental observations with ethyl alcohol, it is expected that splashing is not important for good wetting fluids which fall from one tube to the next under the action of gravity. Splashing of good wetting fluids can be expected only when the liquid is sprayed at high velocity onto the tubes.

3.0 REMARKS ON TUBE ARRANGEMENT

Heat exchanger tube fields are generally laid out with equilateral pitches in either square or triangular arrays. The arrangements are of four basic types: 90°-square; 45°-square; 30°-triangular; and 60°-triangular. With the 30° and 90° arrangements, the transverse pitch (i.e., vertical tube pitch transverse to vapor crossflow) is equivalent to the equilateral pitch, P. This is the case depicted in Fig. 4. With the 60° and 45° arrangements the transverse pitches are $P\sqrt{3}$ and $P\sqrt{2}$ respectively.

Equation (4) for the critical angle and the sketch in Fig. 4 apply only to the 30° and 90° arrangements. Different expressions are needed to calculate the critical angles for the 45° and 60° cases. For the 45° arrangement the critical angle is determined by replacing P with $P\sqrt{2}$ in Eq. (4). For the 60° case the line defining the critical angle is not tangent to the next lower tube, but instead is tangent to a tube in the adjacent column. Thus the critical angle is less than that which would be obtained by replacing P with $P\sqrt{3}$ in Eq. (4). For a given P/D the critical angles for the 45° and 60° arrangements are relatively small compared to the critical angle for the 30° or 90° case. These smaller angles do not necessarily imply a greater potential for deflection because the crossflow velocity is also smaller (in view of the larger transverse gaps).

It is not at all obvious which of the four configurations is superior from a vapor/liquid interaction standpoint. Although a rigorous comparison is dependent on many aspects of each design, a very simple approach can provide some insight into the problem. To establish a basis of comparison, consider four horizontal tube evaporator units, each having a different tube arrangement (i.e., 45°, 90°, 60°, and 30°). Assume that each unit is designed with the same equilateral pitch-to-diameter ratio, P/D, and the overall envelope of each tube bundle is square. Moreover, each unit has an equal number of tubes and hence the same heat duty and total vapor generation. In each unit the vapor is assumed to flow horizontally outward from the vertical centerline. The relative merit of each unit was examined using the droplet and column deflection models. Based on this approach, the 45° arrangement was found to be the best (i.e., least vulnerable to entrainment), followed closely by the 60°, 90°, and 30° arrangements. The relatively high ranking of the 60° configuration is a bit misleading because uniform transverse gap velocity was assumed in the calculations. For the other tube arrangements

this assumption is reasonably good. However for the 60° arrangement the velocity will be non-uniform in view of the large transverse gap and the proximity of tubes in adjacent columns. The crossflow velocity will be negligibly small at a gap location midway between the tubes and relatively large in the neighborhood of the upper and lower tubes. Consequently the deflection of drops and columns is probably underestimated for the 60° configuration. It is quite possible that a more exact analysis would reveal that the 60° arrangement is actually the least desirable insofar as vapor/liquid interaction is concerned.

Although the 30° configuration was found to be somewhat more vulnerable to liquid deflection than the other arrangements, it must be emphasized that the approach used for the comparison is very crude. Furthermore, vapor/liquid interaction is only one of a number of factors that must be considered in the thermal design of evaporators. Thus, on the basis of the foregoing comparison alone, no arrangement should be precluded as a viable candidate.

4.0 SUMMARY AND CONCLUSIONS

A study of vapor/liquid interaction and entrainment in shell-and-tube evaporators was conducted. Attention was focused on horizontal tube falling film evaporators for OTEC. In the horizontal tube design, liquid falls from one tube to the next in either a droplet or column mode. The spacing between droplet generation sites and columns can be predicted by the most unstable wavelength for the Taylor instability.

Based on an experimental study (using ethyl alcohol) of droplet detachment and breakup, a correlation was established for determining the resulting drop sizes. Applying the correlations to ammonia at 22°C (72°F) it was found that 90% of the liquid exists as large droplets of diameter ∿ 5.1 mm (0.20 in.) and 10% is in the form of smaller droplets in the range 1.2 mm (0.05 in.) to 1.9 mm (0.08 in.). The equations of motion were solved to determine the droplet trajectories. With ammonia as the working fluid and P/D = 1.25 (in a 30°-triangular or 90°-square arrangement), it was predicted that vapor crossflow can produce partial or total deflection of droplets away from the lower tubes. To completely avoid deprivation of liquid to the lower tubes and redistribution of the working fluid, the maximum allowable crossflow velocity was calculated to be 1.6 m/s (5.3 ft/sec).

A criterion was derived for predicting the transition from the droplet mode to the column mode. For ammonia transition was predicted to occur at Γ = 0.013 kg/s·m (32 lb/hr·ft). A model was developed for determining the deflection of a column due to vapor crossflow. The maximum allowable velocity was found to depend on the flowrate per unit length, and for P/D = 1.25 increases from 1.5 m/s (5 ft/sec) at the transition flow to 3 m/s (10 ft/sec) at 0.21 kg/s.m (500 lb/hr.ft). In the column mode it was predicted that the percent of the available crossflow area blocked by liquid columns increases from about 8% at the transition flowrate to nearly 30% at 0.21 kg/s·m.

At high vapor velocity liquid can be stripped from the tubes and entrained by the vapor. An inception criterion was presented which predicts a critical vapor velocity of 4.7 m/s (15 ft/sec). (This applies to both horizontal and vertical falling film evaporators.) If an evaporator is designed to satisfy the droplet and column deflection constraints, then

entrainment by stripping will not be a problem.

Other vapor/liquid interaction mechanisms were considered: droplets generated as bubbles burst through the film in the case of boiling and splashing as liquid falls from one tube to the next. Splashing was judged to be insignificant for good wetting fluids such as ammonia. Using Petrovichev's dimensional entrainment correlation which is based on boiling of thin water films, entrainment for ammonia was found to be small. However since the correlation is strictly valid only for water, further work is needed before any conclusive assessment can be made regarding ammonia.

A crude comparison was made of four tube arrangements (30°-triangular, 60°-triangular, 45°-square, and 90°-square) to determine which is superior from a vapor/liquid interaction standpoint. The 45° arrangement was found to be the best and the 60° configuration probably the worst. However in view of the simplicity of this comparison, no arrangement should be precluded as a viable candidate.

The vapor/liquid interaction and entrainment models developed in this paper are general, and should prove to be useful tools for the thermal design and performance evaluation of shell-and-tube evaporators for OTEC.

REFERENCES

1. Bellman, R. and Pennington, R. H., "Effects of Surface Tension and Viscosity on Taylor Instability," Quar. Appl. Math., Vol. 12, 1954, pp. 151-162.

2. Lienhard, J. H. and Sun, K., "Effects of Gravity and Size Upon Film Boiling From Horizontal Cylinders," Journal of Heat Transfer, Trans. ASME, Series C, Vol. 92, No. 2, May 1970, pp. 292-298.

3. Berghmans, J., "Film Boiling Near the Critical State," Int. J. Heat Mass Transfer, Vol. 18, 1975, pp. 1127-1130.

4. Sabin, C. M. and Poppendiek, N. F., "Film Evaporation of Ammonia over Horizontal Round Tubes," Proceedings, Fifth Ocean Thermal Energy Conversion (OTEC) Conference, Miami Beach, Florida, Feb. 1978.

5. Schlichting, H., Boundary Layer Theory, McGraw Hill Book Company, New York, 1968, p. 17.

6. Wallis, G. B., One-dimensional Two-phase Flow, McGraw Hill Book Company, New York, 1969, p. 377.

7. Lamb, H., Hydrodynamics, Dover Publications, New York,1945, pp. 456-457.

8. Yih, C. S., Fluid Mechanics, McGraw Hill Book Company, New York, 1969, pp. 497-498.

9. Ishii, M. and Grolmes, M. A., "Inception Criteria for Droplet Entrainment in Two-Phase Concurrent Film Flow," AIChE J., Vol. 21, No. 2, 1975, pp. 308-318.

10. Kutateladze, S. S., "Elements of the Hydrodynamics of Gas-Liquid Systems," Fluid Mechanics - Soviet Research, Vol. 1, No. 4, 1972, pp. 29-42.

11. ter Haar, D., Collected Papers of P. L. Kapitza, Pergamon Press, New York, 1965, Vol. 2, pp. 662-709.

12. Petrovichev, V. I. et al., "Droplet Entrainment in Boiling of Thin Liquid Films," Heat Transfer - Soviet Research, Vol. 3, No. 1, 1971, pp. 19-22.

13. Newitt, D. M. et al., "Liquid Entrainment: (1) The Mechanism of Drop Formation From Gas or Vapor Bubbles," Trans. Instn. Chem. Engrs., Vol. 32, 1954, pp. 244-261.

14. Snyder, E., "Design of 1 MWe Heat Exchangers for OTEC," Proceedings, Fifth Ocean Thermal Energy Conversion (OTEC) Conference, Miami Beach, Florida, Feb 1978.

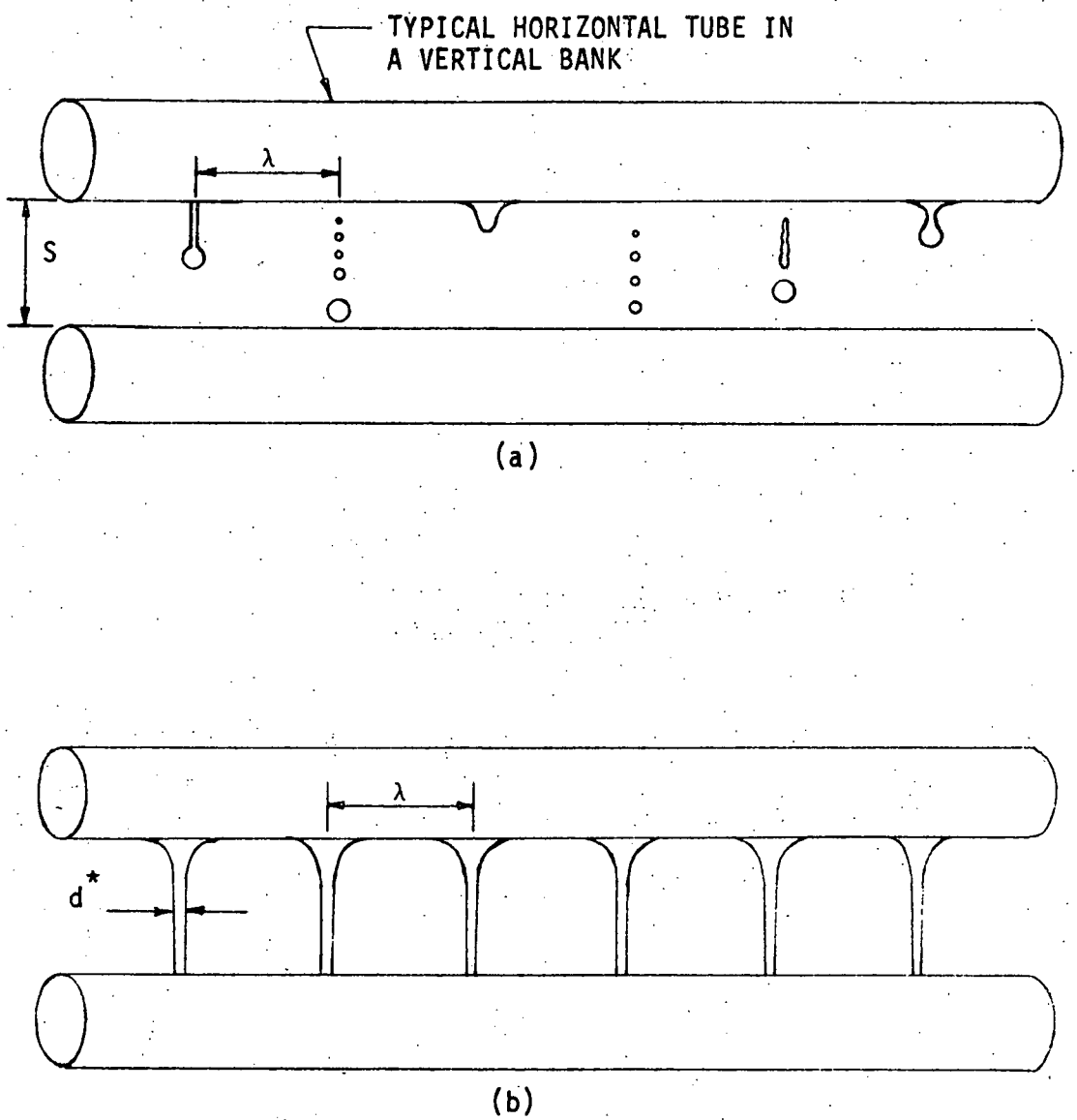

Fig. 1 Liquid falling in (a) droplet mode; and (b) stable column mode.

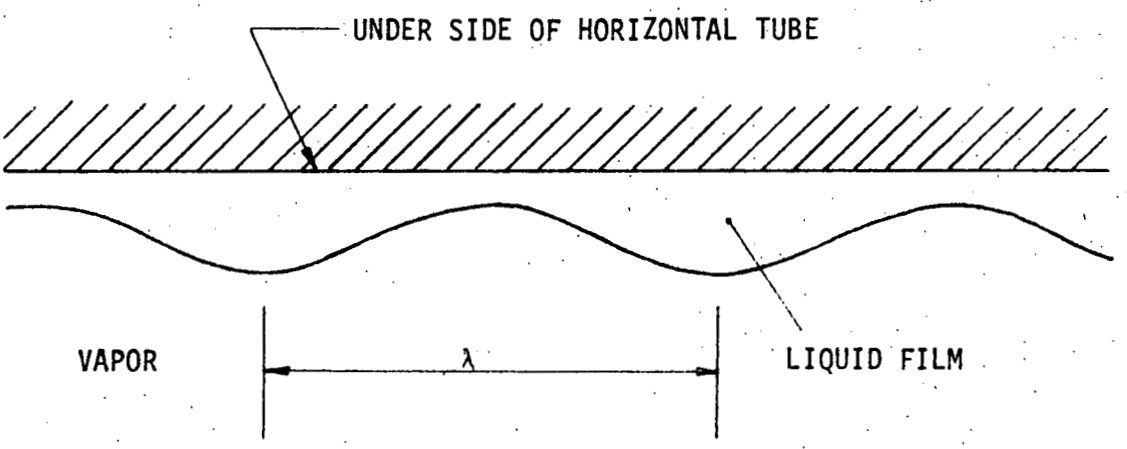

Fig. 2 Taylor instability at liquid/vapor interface.

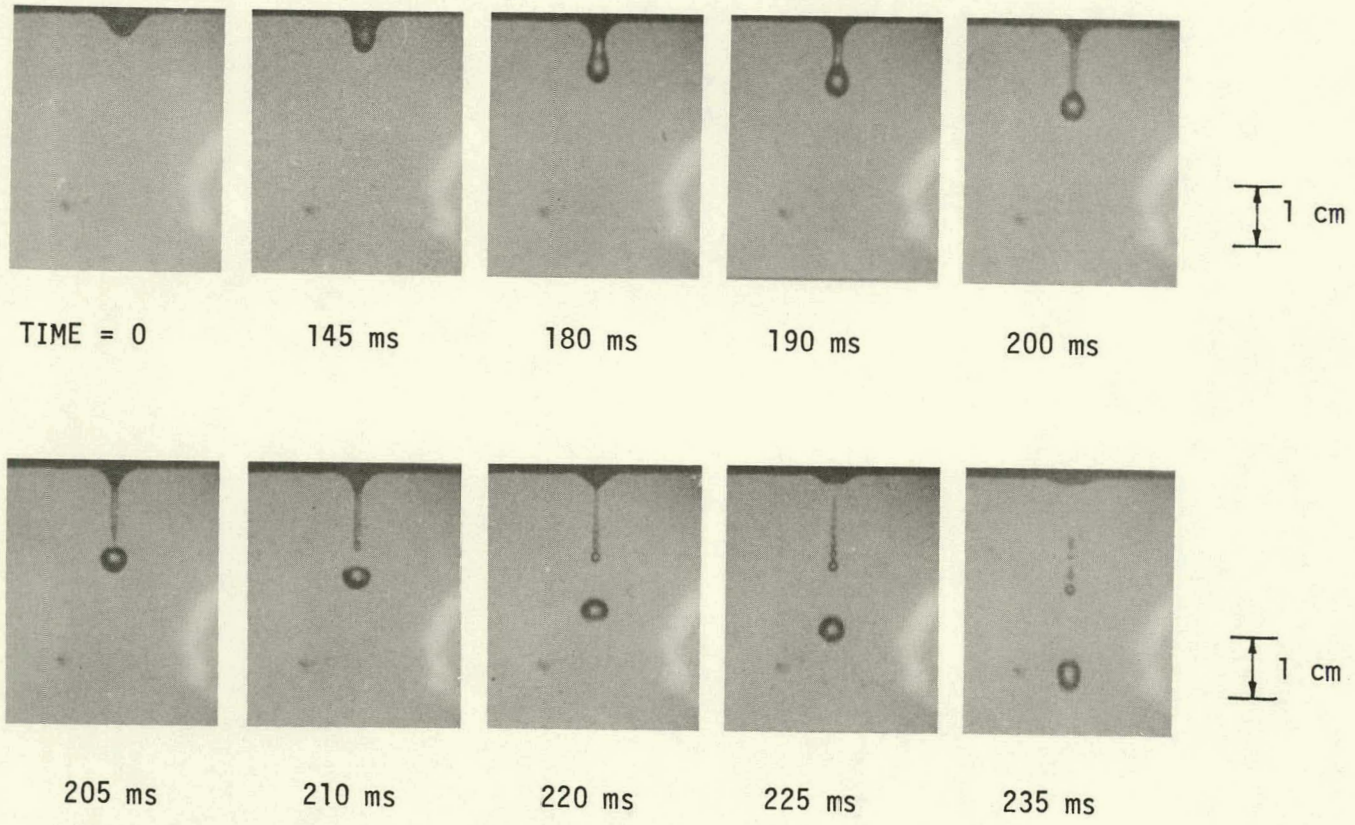

Fig. 3 Movie sequence of a drop detaching from a thin film.

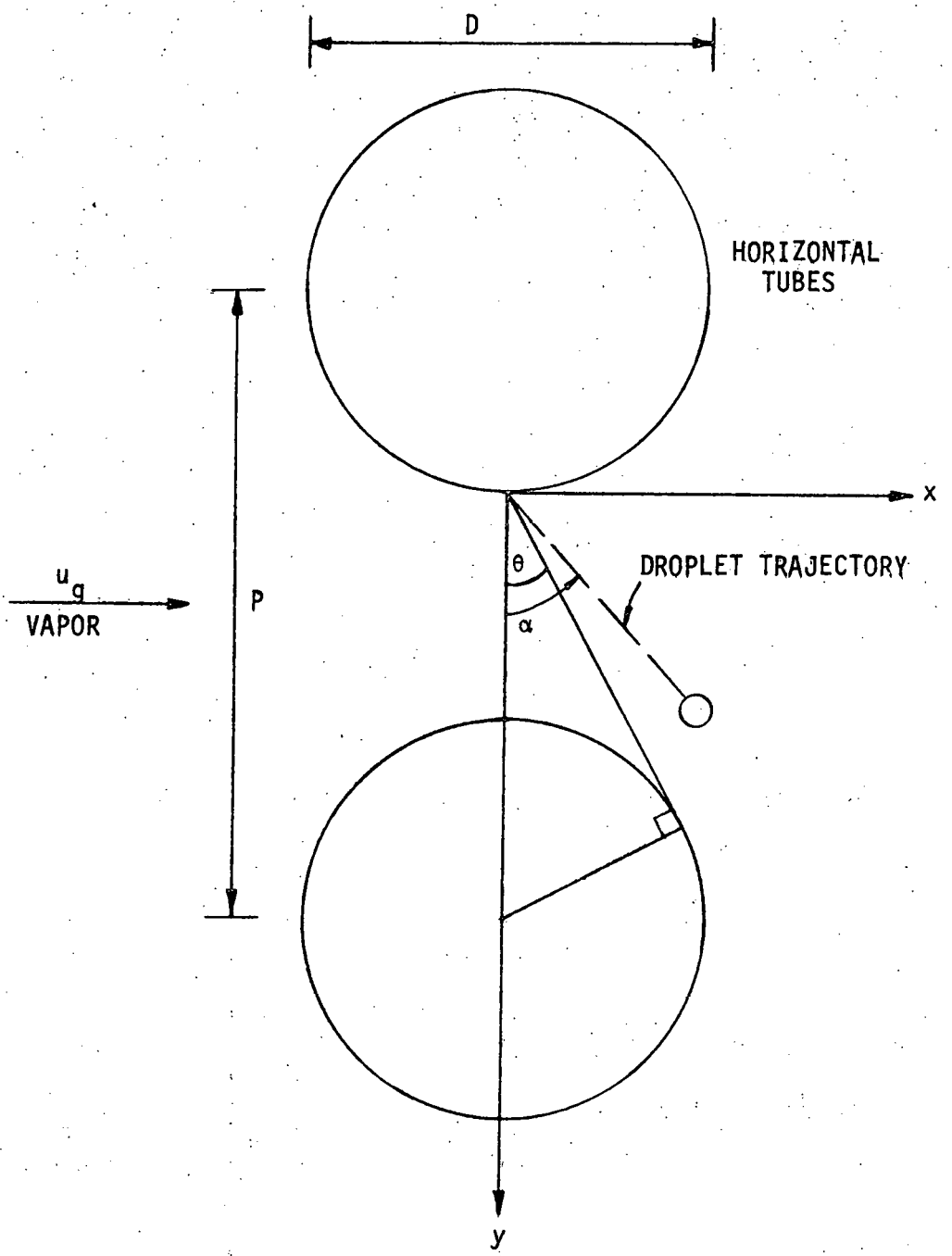

Fig. 4 Deflection of droplet due to vapor crossflow.

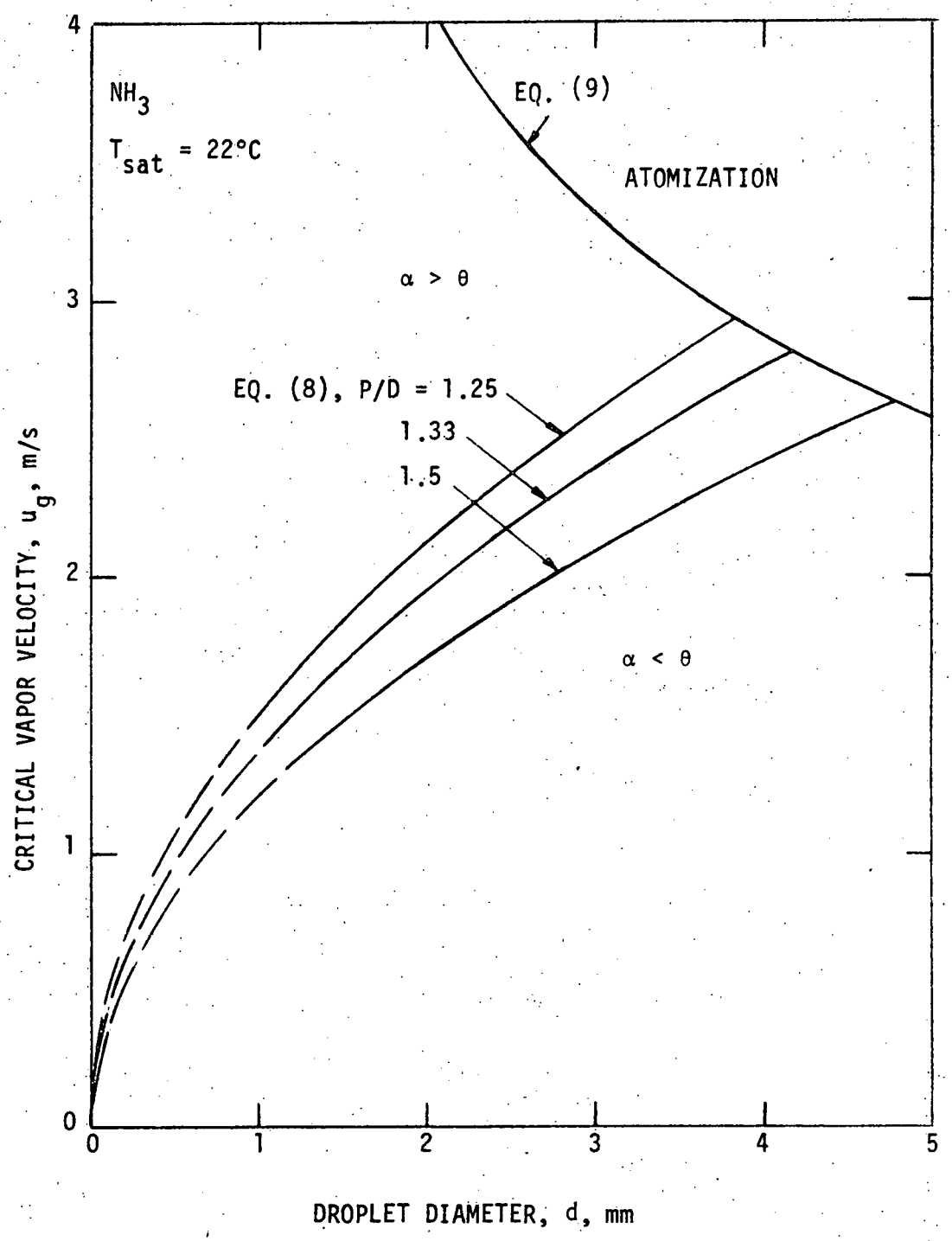

Fig. 5 Maximum allowable crossflow velocity for droplet deflection.

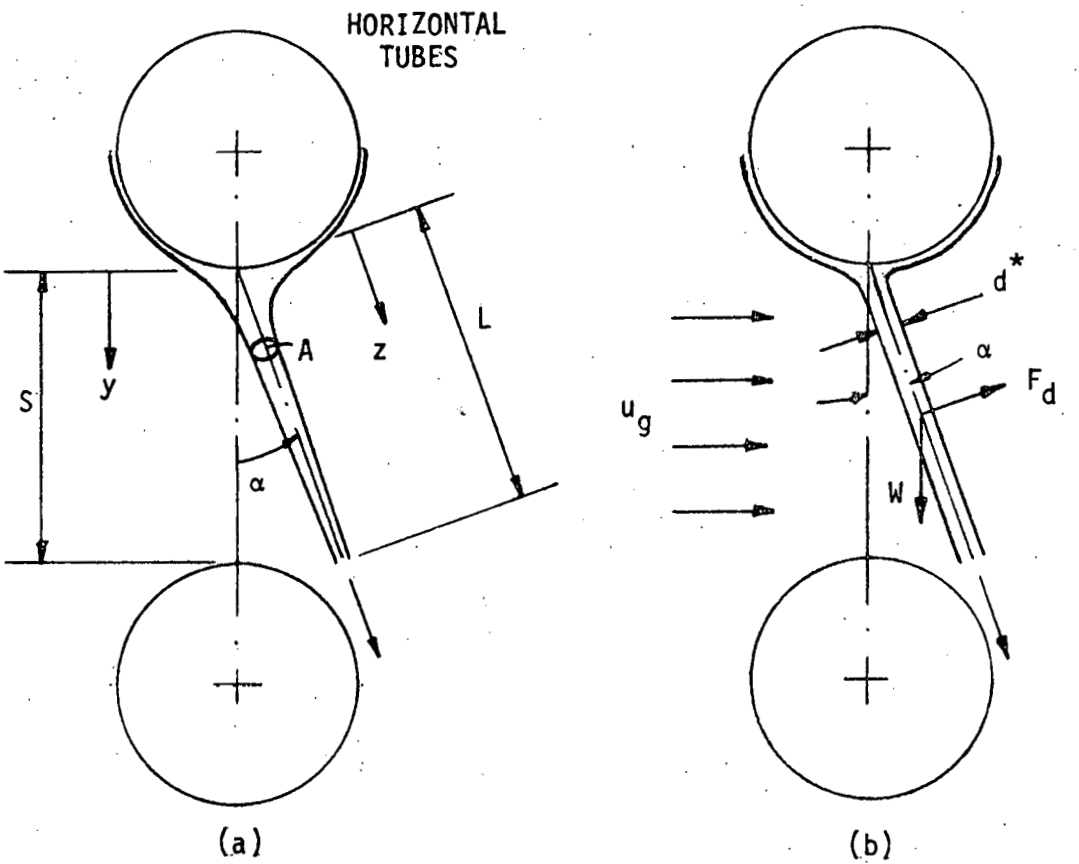

Fig. 6 Deflection of liquid column due to vapor crossflow.

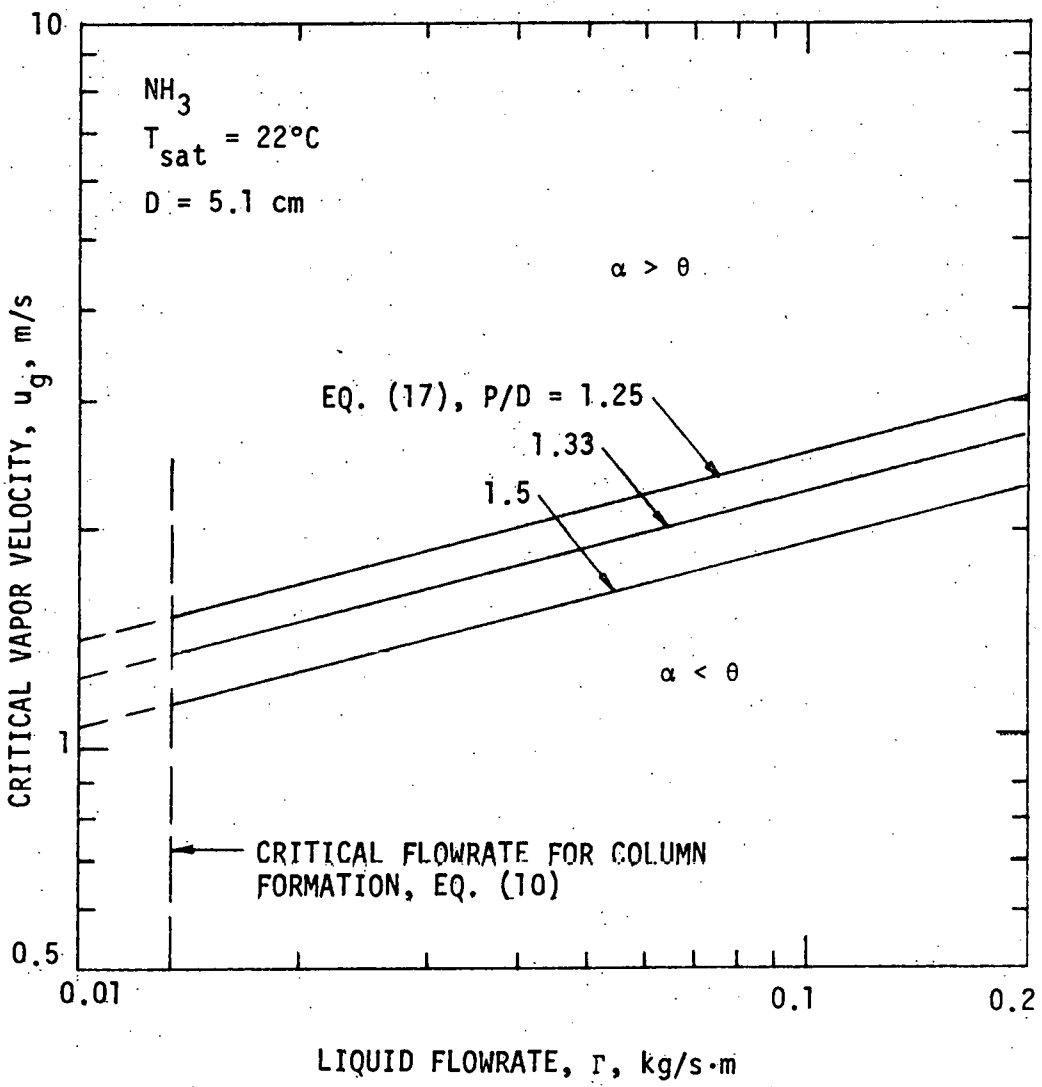

Fig. 7 Maximum allowable crossflow velocity for column deflection.